Agricultural and Forest Meteorology 271 (2019) 285–294

Contents lists available at ScienceDirect

Agricultural and Forest Meteorology

journal homepage: www.elsevier.com/locate/agrformet

Use of thermal imaging to detect evaporative cooling in coniferous and broadleaved tree species of the Mediterranean maquis

Omri Lapidot[a], Timea Ignat[b], Ronit Rud[b], Ido Rog[a], Victor Alchanatis[b], Tamir Klein[a,*]

[a] Department of Plant & Environmental Sciences, Weizmann Institute of Science, Rehovot, Israel
[b] Agricultural Engineering, ARO Volcani Center, Bet Dagan, Israel

ARTICLE INFO

Keywords:
Evaporative cooling
Thermal imaging
Transpiration rate
Leaf gas exchange
Conifers
Broadleaves

ABSTRACT

Among forest types, the Mediterranean maquis is specifically exposed to fluctuations in water availability. Therefore, monitoring the water-use patterns of its major tree species is key in quantifying the local and regional water balance. However, the traditional measurement methods of tree water-use at high spatial scales are difficult and labor-intensive, thus indirect methods become useful. Evaporation of water from the stomatal pores on the leaf surface involves evaporative cooling, and hence the differences between the leaf temperature and its surrounding air temperature ($\Delta T_{leaf\text{-}air}$) can serve as a reliable estimator for tree water-use.

Here, we used direct measurement of transpiration rate (E) with a gas exchange system, simultaneously with ground Thermal Infra-Red (TIR) imaging to study the relationship between $\Delta T_{leaf\text{-}air}$ and E in dominant tree species of the Mediterranean maquis. Controlled experiments were conducted in parallel with measurements in the forest, on five tree species of contrasting leaf shapes (Conifers: *Pinus halepensis*; *Cupressus sempervirens*; Broadleaf: simple: *Quercus calliprinos*; *Ceratonia siliqua*; compound: *Pistacia lentiscus*). Next, we used a quantitative approach, applying a leaf energy balance model to estimate E from the TIR images and compared it to the direct measurement of the gas exchange system.

We report evaporative cooling across the five species, replicated in tree saplings and in mature trees in the forest. The conifers were significantly cooler than broadleaves by up to ~4 °C and produced narrower $\Delta T_{leaf\text{-}air}$ ranges. Estimations of E from $\Delta T_{leaf\text{-}air}$ were relatively close to the observed E, with some overestimations. Our observations show that TIR imaging can detect transpiration-related differences in $\Delta T_{leaf\text{-}air}$ among species and can be used to estimate E in natural environments. Yet, the dependence of $\Delta T_{leaf\text{-}air}$ on E is species-specific and thus, empirical associations must be developed separately for each of the species.

1. Introduction

The Mediterranean maquis is a widely distributed ecosystem around the Mediterranean basin, characterized by mixed, densely growing forests. Typically, the Mediterranean maquis is populated by sclerophyllous, mostly evergreen, but also deciduous, trees and shrubs (Danin, 1988). The functioning of the Mediterranean maquis is heavily influenced by air temperature and soil water content and is vulnerable to climate change, mainly due to fluctuations in water availability, accompanied by a complex topography in many sites (Lavorel et al., 1998). In fact, the Mediterranean basin was predicted to be affected by global climate change more than any other region on Earth (Giorgi, 2006). Climate projections estimate future increases in air temperature, declines in precipitation, and extended dry periods (Goubanova and Li, 2007), producing a negative soil water balance and limited water supplies (Lavorel et al., 1998).

The Mediterranean vegetation has adopted various strategies to cope with water stress and survive under drought conditions, from root extension to leaf stomatal regulation. During the dry summer, isohydric-like species, such as *Pinus halepensis*, a coniferous tree with a relatively shallow root system, reduce their stomatal conductance to keep a constant minimum leaf water potential, which limits leaf transpiration and thereby helps to minimize water loss (Klein et al., 2011). In contrast, species with anisohydric-like behavior, such as *Quercus calliprinos*, a broadleaf tree with a relatively deep root system, maintain leaf transpiration by keeping their stomata open during the day and thereby ensuring continuous carbon uptake, metabolism and growth under drought conditions (Klein et al., 2013). Such a difference in water-use strategy affects water availability at multiple spatial and temporal scales.

* Corresponding author at: Department of Plant & Environmental Sciences, Weizmann Institute of Science, 76100, Rehovot, Israel.
E-mail address: tamir.klein@weizmann.ac.il (T. Klein).

https://doi.org/10.1016/j.agrformet.2019.02.014
Received 25 September 2018; Received in revised form 18 January 2019; Accepted 9 February 2019
0168-1923/ © 2019 Elsevier B.V. All rights reserved.

Tree water-use is a continuous process, from root water uptake through xylem transport, up to leaf transpiration. In the process of transpiration, latent heat of evaporation, i.e. the energy required to convert water from liquid phase to gas phase, is released from the leaf in the evaporating water and cools it down (Gates, 1968). As a result, there is an inverse proportional relationship between E and leaf to air temperature differences ($\Delta T_{leaf\text{-}air}$) and hence $\Delta T_{leaf\text{-}air}$ can serve as a reliable indicator for E, stomatal conductance (g_s), and plant water status (Fuchs, 1990; Campbell and Norman, 1990; Inoue et al., 1990, 1994; Jones, 1999a, b; Leinonen et al., 2006; Lima et al., 2016). Previous studies have found that evaporative cooling has a significant role in promoting over-heating avoidance (Schymanski et al., 2013), survival under drought stress and extreme heat conditions (Urban et al., 2017) and in keeping the leaf temperature (T_L) within the optimal temperature ranges for enzyme function (Burke and Upchurch, 1989). Knowledge of evaporative cooling effect on leaves has been used in surveys of canopy temperature in agriculture for plant water status evaluation, as part of irrigation scheduling since the 1960′s (Tanner, 1963; Fuchs and Tanner, 1966). A number of indices for estimating water status in crops based on thermal measurements were developed, such as crop water stress index (CWSI; Idso et al., 1981; Jackson et al., 1981) and the I_g index (Jones, 1992), which quantify plant drought stress and stomatal conductance, respectively. Canopy temperature, obtained by thermal measurements, is affected by canopy architecture (e.g., foliage density, leaf cover, branching; Scherrer et al., 2011) and leaf characteristic (e.g., leaf width, shape, angle; Jarvis and McNaughton, 1986; Bridge et al., 2013). These factors influence the coupling of foliage to the air stream, and hence increases in leaf size and canopy density typically result in an increase in T_L. Thus, 40-m tall coniferous species showed cooler canopy temperatures than equally sized broadleaved species (Leuzinger and Körner, 2007).

Traditional field measurement methods for T_L, E, and g_s involve direct-contact measurement at the leaf surface, e.g. using a thermocouple-equipped infra-red gas analyzer (Klein et al., 2013). This method is considered difficult for execution on a large number of leaves, often with significant errors due to the limited number of replications. The improvement in infra-red imaging technologies, together with satellite and unmanned aerial vehicle developments, enable high resolution, large scale surveys, as demonstrated in a temperate mixed forest (Scherrer et al., 2011). This method is considered non-harmful and non-invasive and therefore, it does not affect tree leaf function. It can be applied at different scales (from a single leaf, through a whole-tree crown, to a forest canopy) and more importantly, it allows for collection of information over a large number of trees over a short time.

Although thermal remote sensing studies for canopy temperature of forest tree species have already been done in the past (Leuzinger and Körner, 2007; Scherrer et al., 2011; Reinert et al., 2012; Aubrecht et al., 2016; Kim et al., 2016), little is known about $\Delta T_{leaf\text{-}air}$ distributions in the relatively low-stature tree species of the Mediterranean maquis. More importantly, despite the great potential of using thermal imaging to capture $\Delta T_{leaf\text{-}air}$ dynamics and estimate water status at canopy scale (Jones et al., 2004; Cohen et al., 2005; Möller et al., 2007; Alchanatis et al., 2010; Meron et al., 2013), applications to forest canopies have been very limited.

The objectives of this study was to study the dynamics between E and $\Delta T_{leaf\text{-}air}$ on five key Mediterranean tree species of contrasting leaf shapes (conifers vs. broadleaved) and to evaluate the use of TIR imaging in transpiration-related differences among species. We hypothesized that (1) in and across tree species, $\Delta T_{leaf\text{-}air}$ and E are inversely correlated; (2) $\Delta T_{leaf\text{-}air}$ of coniferous species should be lower than that of broadleaved species; and (3) the indirect, thermography-based estimation of E should demonstrate relatively close agreement with the direct gas exchange measurements of E. Thus, $\Delta T_{leaf\text{-}air}$ measured using TIR imaging can be applied for a rapid, large-scale tree water-use sensing. In turn, TIR thermography will enable testing hypotheses about the level of species competition over water sources, as well as tree species impact on forest eco-hydrology, in service of sustainable forest management.

2. Materials & methods

Our study was conducted on five Mediterranean tree species, with mature trees growing in a mixed forest site and with 1-year-old saplings, of the same five species, growing in a greenhouse. Key Mediterranean tree species were selected based on their contrasting leaf shape and stomatal regulation behavior. Among the selected broadleaves, *Quercus calliprinos*, characterized by anisohydric stomatal response, maintains stomatal conductance at leaf water potential $\Psi_l < -4.0$ MPa (Klein et al., 2013). In contrast, *Pistacia lentiscus* and *Ceratonia siliqua* are characterized by isohydric-like stomatal response, with less negative midday values of leaf water potential, -2.1 MPa and -1.8 MPa, respectively (Trifilò et al., 2015). Among the coniferous species, *Pinus halepensis* is characterized by isohydric-like stomatal response, closing stomata at needle water potential of -3.1 MPa (Klein et al., 2011). In contrast, the threshold for stomatal closure in the anisohydric *Cupressus sempervirens* is at lower water potential of -4.5 MPa (Froux et al., 2005). Since the five species diverge by genera, we name them by their genus throughout the text.

2.1. Field study site

Harel forest is located at the Judean foot hills (31° 43′N 34° 57′E, 320 m elevation), 4 km south-west of Beit Shemesh, Israel. The first generation of trees was planted in the 1930′s. The vegetation is dominated by oak (*Quercus*) and pine (*Pinus)*. The soil is composed of a brown rendzina layer overlaying hard chalky soil and occasionally hard lime stone. This forest soil is reach in organic matter and characterized by a high water-holding capacity and low desiccation rates, allows the tree's root environment a continuous water uptake after rain events (Singer, 2007). This area is characterized by a Mediterranean climate regime with mean annual temperature of 20 °C and 490 mm annual precipitation (Klein et al., 2013). A previous study by Klein et al. (2013), in the same experimental plot showed relatively low rates of transpiration and photosynthesis and also high ratio between CO_2 assimilation and stomatal conductance (intrinsic water-use efficiency; WUEi), indicating water stress and low activity levels during the dry period (May-Oct), in contrast to the high activity levels that were demonstrated during the wet period (Nov-Apr). Therefore, in order to study dynamics of E and $\Delta T_{leaf\text{-}air}$ between the different tree species, measurements were conducted in two field days during March 2018, when both air temperature and water availability were relatively high (see soil parameters). A total of twenty trees (four individual trees per tree species × five tree species) were labeled for repeated TIR image capture and gas analyzer measurements. Three cycles of measurements were conducted: first between 9:00-11:00 (morning), second between 11:00 - 13:00 (midday) and third between 13:00-15:00 (afternoon). In each measurement cycle, a single leaf per individual tree was measured (see measurement details below). Mature trees' heights ranged between 1.7–2.4 m in *Pistacia*, 3.7–5.5 m in *Quercus,* 6.5–7.6 m in *Ceratonia*, 11.1–14.2 m in *Cupressus*, and 14.5-21.5 m in *Pinus*.

2.2. Tree sapling experiment

One-year old tree saplings of the five Mediterranean tree species were obtained in December 2016 from the Jewish National Fund, Israel's Forest Services (KKL). Trees were grown from seed in plastic containers of 200 mL plugs (5 × 5 cm). To avoid planting shock, trees were kept in the nursery containers during the 45 days prior to measurement. The trees were grown under sustained irrigation regime (watering to field capacity once every two days) and natural light regime in a glass greenhouse located at the Weizmann Institute of Science, Israel. The measurements were conducted during two

measuring days, outside the greenhouse. In order to evaluate differences between species, measurements were carried out at midday, when E is at its maximum (based on preliminary experiments) and because midday was found to be optimal time for TIR imaging (Alchanatis et al., 2010). On 12 January 2017, one gas exchange measurement cycle was conducted between 12:00 and 13:00 on 3 individual trees per species, simultaneously with TIR image acquisition (below). On 16 January 2017, one gas exchange measurement cycle was conducted between 12:00 and 15:00 on 6 individual trees per species. Sapling height differed among the species: 81-141 cm in *Cupressus*, 59-92 cm in *Pinus*, 34-46 cm in *Pistacia*, 20-44 cm in *Ceratonia*, and 12–36 cm in *Quercus*. Yet, these height differences were eliminated for the purpose of capturing all saplings in a single TIR image (below).

2.3. TIR image acquisition

TIR images were taken in the field using a FLIR T1030sc camera (FLIR Systems Inc., Wilsonville, OR, USA), with14-bit, 1027 × 768-pixel resolution, 30 frame rate per second, accuracy of ± 1 °C or 1% of the temperature reading between 5 °C to 150 °C, 7.5–14 μm spectral range, 24.6 mm focal length, 21° x 28° field of view and built-in 5Mpixel digital camera, adapted to the IR lens (technical data taken from the manufacturer). In every image acquisition round in the forest, the camera was placed in a fixed position at a known distance from each tree. Although it may not provide the most representative images of the whole canopy temperature, it allows to capture the maximal sunlit region of the tree crown. Thermal images of *Pistacia* were captured at an average distance of 4.6 m, horizontally to the objects. Images of *Quercus* and *Ceratonia* were captured at an average distance of 7.2 and 8.4 m in elevation angle of 22° and 33°, respectively. Both *Pinus* and *Cupressus* were captured at an average distance of 7 m in angle of 56°. The camera was set to capture thermal and visual images at same time. A total of 120 thermal images were captured. In the tree sapling experiment, TIR images were taken using FLIR sc655 camera (FLIR Systems Inc., Wilsonville, OR, USA), with a 16-bit, 640 × 480-pixel resolution, 50 Hz frame rate, accuracy of ± 2% of the temperature reading, 7.5–13 μm spectral range, 24.6 mm focal length and 25° x 19° field of view (technical data taken from the manufacturer). This model does not have a built-in digital camera. All tree saplings were placed together on a mobile, 79.5 × 110.5 cm wood platform (Fig. 5A). Due to their lower stature, *Ceratonia, Pistacia* and *Quercus* trees were placed on an additional, 45 cm tall plastic platform, to minimize shading by taller trees and to ensure similar distance from the camera. In order to avoid optical errors related to changes in the angles between the object's surface and the IR sensor (i.e. the view angle) relative to the sunlight, the platform was rotated 90 degrees clockwise and faced a different cardinal direction for each of the four total TIR images taken at one minute intervals. The camera was placed vertically to the ground, at a height of 2.8 m above the tree canopy, using a telescoping camera mast, yielding a resolution of 0.43 cm pixel^{-1}.

2.4. Image processing and data analysis

TIR images were processed using FLIR ResearchIR Max software (FLIR Systems Inc., Wilsonville, OR, USA). Image parameters of relative humidity and air temperature were set for each image, based on the measurements from the meteorological station. The emissivity was set to a value of 0.98, as recommended by Idso et al. (1969). TIR Images of mature trees in the forest, were saved as 8-bit gray-level TIFF images and each image was aligned to its matching visual image using the Fiji package for image processing (Schindelin et al., 2012) so that both types of images had corresponding pixels and the same dimensions. For each image, regions of interest (ROI) of similar size (2500 pixels) were manually selected from the center of sunlit leaf areas that included the leaves used for gas exchange measurements. The selection of sunlit leaves was done to avoid observed cooling due to self-shading. The ROI pixels were converted to binary mask and were applied on the TIR images. The gray-level values were converted to temperature values as described in Cohen et al. (2005):

$$T(x, y) = T_{min} + \frac{T_{gray}}{255}(T_{max} - T_{min}) \quad (1)$$

where $T_{(x,y)}$ is the temperature that calculated at the specific pixel (x,y). T_{gray} is the gray level intensity of the specific pixel, ranged from 0 to 255. T_{min} and T_{max} are the minimal and maximal values of temperatures scale in the image, corresponded to the gray levels of 0 (black) and 255 (white), respectively. For all TIR images, T_{min} and T_{max} were set to 15 °C and 40 °C, respectively. TIR images of tree saplings, were saved as comma-separated value (CSV) files, where every cell contains one temperature value per pixel. The ROI pixels were selected from species' sunlit leaves in the central region of the foliage. To overcome the problem of mixed pixels, crown temperatures were separated from background and cold artifacts by setting the lower threshold to 10 °C below air temperature and the higher limit to 7 °C above air temperature, as suggested in Meron et al. (2013). Mean and median of $\Delta T_{leaf\text{-}air}$, skewness (i.e. the asymmetry of distribution) and kurtosis (i.e. the thickness of the tails of distribution) were calculated.

2.5. Thermography-based transpiration rate estimation

Calculation of E is based on the leaf energy flux balance, in which leaf temperature is dependent on the balance between the absorbed solar radiation and heat loss by transpiration and convection (Jones, 1992):

$$\frac{T_{Leaf}}{dt} = R_{net} + M - G - \lambda E - H \quad (2)$$

where R_{net} is net radiation absorbed (W m^{-2}), M is metabolic heat generated from photosynthesis and respiration (usually less than 1%, so neglected), G is heat flux to soil (W m^{-2}, assume not relevant to canopy leaves), λ is latent heat of vaporization of water (J mol^{-1}) and H is the sensible heat loss by convection and conduction to the environment.

In steady state, the mean one-sided value of E can be written as:

$$E = (R_{net} - H)/2\lambda \quad (3)$$

The sensible heat flux (H) is derived from the temperature difference between the leaf and the air, $\Delta T_{leaf\text{-}air}$, and defined as:

$$H = C_p * G_{HR} * \rho * (\Delta T_{leaf\text{-}air}) = C_p * (G_{bH} + G_R) * \rho * (\Delta T_{leaf\text{-}air}) \quad (4)$$

where C_p is the specific heat of air, ρ is the air density, G_{HR} is the boundary layer conductance ($G_{HR} = G_{bH} + G_R$), G_{bH} is the boundary layer conductance to heat transfer (mm s^{-1}) and G_R is the radiative transfer conductance (can be calculated in $G_R = 4 * \varepsilon * \sigma * Tair^3 / \rho * C_p$. where ε is emissivity and σ is Stefan-Boltzmann constant).

A similar equation for non-transpiring leaf (T_{dry}) takes the following shape:

$$H = C_p * (G_{bH} + G_R) * \rho * (\Delta T_{dry\text{-}air}) \quad (5)$$

where $\Delta T_{dry\text{-}air}$ is the temperature difference between the non-transpiring leaf and the air. Condensing Eqs. (3),(4) and (5) into a single equation yields:

$$E = C_p * \rho * (G_{bH} + G_R) * (T_{dry\text{-}Leaf}) / \lambda \quad (6)$$

where $\Delta T_{dry\text{-}Leaf}$ is the temperature difference between a transpiring and a non-transpiring leaf and G_{bH} can be calculated for flat plane leaves in (Jones, 1992):

$$G_{bH} = 6.62 * (u/d)^{0.5} \quad (7)$$

G_{bH} for coniferous leaves would be:

$$G_{bH} = 4.03 * (u^{0.6}/d^{0.4}) \quad (8)$$

Where u is wind speed (m s^{-1}) and d is characteristic leaf width (m). Based on previous studies (Irmak et al., 2000; Cohen et al., 2005; Jones et al., 2018) T_{dry} was approximated as $T_{air}+5$ °C. Based on our forest measurements, we assume $T_{dry} = T_{air}+1$ °C for *Pinus*. In addition, we assume characteristic leaf width of 0.0015 m for *Pinus*, 0.003 m for *Cupressus,* 0.02 for *Pistacia,* 0.03 for *Quercus* and 0.04 for *Ceratonia*.

2.6. Leaf gas exchange measurements

Rates of leaf transpiration (E, mmol H_2O m^{-2} s^{-1}), stomatal conductance (g_s, mol H_2O m^{-2} s^{-1}) and net assimilation (A, μmol CO_2 m^{-2} s^{-1}) were measured in the field using the portable gas exchange system GFS-3000 (Heinz Walz GmbH, Effeltrich, Germany). The sensor head was equipped with a red-blue LED light source inside a standard leaf chamber (8 cm^2). For each measurement cycle, we set the light intensity inside the leaf chamber to the level measured outside the chamber, so the measured rate of E, A and g_s reflected the leaf's rates at ambient conditions. The light level inside the leaf chamber was adjusted and kept constant for each measurement cycle to exclude light-induced differences that typically occur when using the open-top chamber. The CO_2 mixer was set to provide a stable concentration of 400 ppm as in the outside atmosphere, and flow rate was set to 750 μmol s^{-1} inside the sample chamber. In each measurement, a single, sunlit, mature leaf from the broadleaved trees, or a needle cohort of 10 adult needles from the conifers was randomly sampled. Subsequently, the leaves were cut and transferred to the lab for leaf area calculation using a flatbed scanner HP color jet pro MFP m477fdn. The leaves were scanned under background of A4 (210 x 297 mm) white paper and their area was calculated using Fiji package for image processing (Schindelin et al., 2012). The measured area was separated from the background with the color threshold tool and then calculated using the particle analyzer tool. Leaf area differed among the species: 5.59 ± 0.16 cm^2 in a needle cohort of 10 adult needles of *Pinus*, 4.2 ± 0.22 cm^2 in *Cupressus*, 4.77 ± 0.25 cm^2 in *Pistacia*, 6.26 ± 0.29 cm^2 in *Quercus* and 12.7 ± 0.94 cm^2 in *Ceratonia*. All gas exchange parameters were calculated per projected leaf area. In addition, gas exchange measurements were used to calculate the intrinsic water-use efficiency at the leaf level (WUEi, μmol CO_2 mol^{-1} H_2O) according to:

$$\mathrm{WUEi} = \frac{A}{g_s} \tag{9}$$

In the tree sapling experiment, the gas exchange measurements followed the same protocol using a Li-6400 Portable Photosynthesis system (LI-COR Biosciences, Lincoln, NE, USA). During the measurement, T_L of the enclosed leaf was detected by a fine-wire thermocouple sensor, located inside the leaf measurement chamber. These provide accurate temperature measurement (Smigaj et al., 2017; Kim et al., 2018) and real-time evaluation of the effect of E on T_L in leaf-scale.

2.7. Meteorological data

The meteorological information was provided by the Israel Meteorological Services (IMS). Air temperature and relative humidity were measured at standard height of 2 m at Beit Jimal weather station, located 1.4 km from our measured forest plot. These values were in good agreement with values measured on site (Fig. S1). Expectedly, air temperature under the forest canopy was ~2 °C warmer than at the exposed weather station, yet this difference was consistent. Wind direction and speed were measured at standard height of 10 m at Netiv Ha Lamed Hei weather station, located 4.5 km from the plot. Both weather stations provide 10-minutes averaged observations. Vapor pressure deficit (VPD, Pa) was calculated based on air temperature (T_{air}, °C) and relative humidity (RH, %) according to:

$$\mathrm{VPD} = \left(1 - \left(\frac{\mathrm{RH}}{100}\right)\right) * 610.7 * 10^{7.5\mathrm{Tair}/(237.3+\mathrm{Tair})} \tag{10}$$

In the tree sapling experiment, which was conducted outside the greenhouse at the Weizmann institute of Science, meteorological information of air temperature, relative humidity, wind direction and speed was provided by a portable weather station (Campbell Scientific Inc., Logan, UT, USA) at a standard height of 2 m above ground.

2.8. Soil water parameters

Soil moisture content (%, v/v) and soil water potential (MPa) were measured using a dielectric constant EC-5 soil moisture sensor and an MPS-6 soil water potential sensor, respectively (Decagon devices Inc., Pullman, WA, USA). In the mature tree measurements, the sensors were located in the center of the measured forest plot at 3 depths: 5, 25 and 35 cm below ground surface. The sensors were connected into an Em50 Data logger (Decagon devices Inc., Pullman, WA, USA), which was programmed to record observations at 30 min intervals.

2.9. Statistical analysis

All the raw data analysis, statistical computing and graphics, were done using R statistical software (R Core Team, 2013). Due to the similarity in soil and meteorological conditions and in the daily gas exchange patterns, an average values from these two measuring days is represented. Because the leaf temperature distributions violate normality and equality of variances assumptions, non-parametric tests were used. Differences in T_L between tree species were evaluated by performing a Kruskal-Wallis test and comparison between leaf types was evaluated by Welch's *t*-test with significance level of 0.05. Due to the fact that meteorological data were provided by two independent weather stations, correlation between them was tested by Pearson's correlation coefficient. In order to evaluate the utility of the leaf energy balance model, a comparison between gas exchange measurements and thermography-based estimations of E was performed by calculating the mean absolute error (MAE). MAE was chosen over other error terms (e.g. mean root squared error), because of its lower sensivity to extreme values.

3. Results

3.1. Leaf temperature and transpiration in mature trees in the forest

Leaf gas exchange of mature trees in the Harel forest was measured during two meteorologically similar days on 20 and 26 March 2018, a time of the growing season when soil water content is still relatively high and transpiration is not restricted. Soil moisture was stable along the day with a daily average of 10.92 ± 0.03, 6.34 ± 0.02 and 8.11 ± 0.01% v/v in 5, 25 and 35 cm depth respectively in the first day (data not shown). Same patterns were recorded in the second day of measurements, with 12.09 ± 0.02, 7.3 ± 0.02 and 8.36 ± 0.01% v/v, respectively. Soil water potential measurements also showed small variations throughout the day with a daily average of -2.94 ± 0.02 and -1.96 ± 0.00 MPa in 5 and 25 cm depth, respectively on the first day and -1.81 ± 0.03 and -1.95 ± 0.00, respectively, on the second day (data not shown).

Mean (n = 8) gas exchange parameters (E, g_s and WUEi) along daytime showed large differences among tree species (Fig. 1). *Cupressus* and *Quercus* showed similar E patterns with the maximum at midday (2.10 ± 0.33 and 1.04 ± 0.13 mmol H_2O m^{-2} s^{-1}, respectively; Fig. 1A). In contrast, *Ceratonia, Pistacia,* and *Pinus* showed a decrease in E from 2.62 ± 0.34, 2.35 ± 0.39 and 1.90 ± 0.22 mmol H_2O m^{-2} s^{-1} during morning hours to 1.41 ± 0.24, 1.56 ± 0.37 and 0.93 ± 0.14 mmol H_2O m^{-2} s^{-1} during afternoon hours, respectively. A reduction in g_s throughout the daytime was observed in all species (Fig. 1B). This decrease in g_s followed an increase in VPD of 1–2 kPa from morning to midday hours (Fig. S2, S3). The isohydric-like tree species, *Ceratonia*, showed the sharpest decrease in g_s with

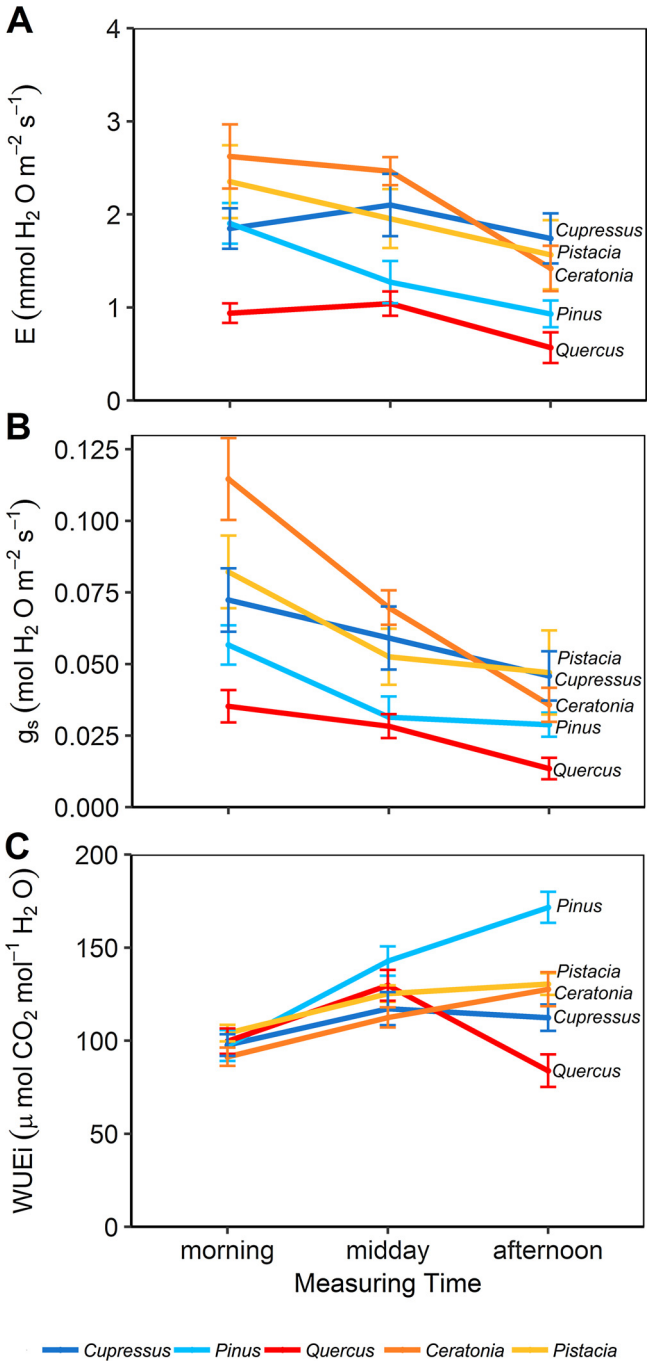

Fig. 1. Gas exchange parameters of five Mediterranean tree species in the Harel forest. Mean ± SE (n = 8) rates of (A) Transpiration rate, (B) Stomatal conductance, (C) Intrinsic water use efficiency of mature trees. The different colours represent different tree species (*Cupressus sempervirens, Pinus halepensis, Quercus calliprinos, Ceratonia siliqua, Pistacia lentiscus*).

-0.079 ± 0.014 mol H_2O m^{-2} s^{-1} from morning hours to afternoon. In contrast, the anisohydric-like tree species, *Quercus,* showed a stable and moderate decrease in g_s with -0.022 ± 0.008 mol H_2O m^{-2} s^{-1} from morning hours to afternoon. The tree species (aside from *Cupressus* and *Quercus*) showed continuous increase in WUEi throughout the day (Fig. 1C). WUEi ranged between 91 and 104 μmol CO_2 mol^{-1} H_2O during the morning and between 84 to 172 μmol CO_2 mol^{-1} H_2O during afternoon. Overall, the isohydric-like tree species *Ceratonia, Pinus* and *Pistacia* had higher mean WUEi (110.51 ± 4.85, 137.27 ± 7.81 and 120.62 ± 3.55, respectively) than the anisohydric-like tree species,

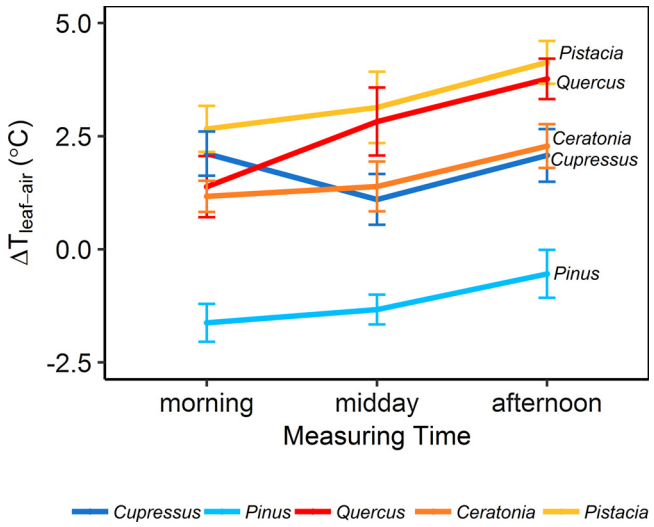

Fig. 2. Daytime variations in $\Delta T_{leaf\text{-}air}$ for sunlit leaves of the five tree species in the Harel forest. The error bars represents the standard error of the mean (n = 8).

Cupressus and *Quercus* (85.29 ± 4.71 and 86.6 ± 5.78).

All tree species aside from *Cupressus* showed a continuous increase in $\Delta T_{leaf\text{-}air}$ from morning to afternoon (Fig. 2). This increase in $\Delta T_{leaf\text{-}air}$ followed a decrease in E and g_s throughout the day (Fig. 1A and 1B). In contrast, *Cupressus* showed absolute minimum in $\Delta T_{leaf\text{-}air}$ at midday, followed by an absolute maximum in E (Fig. 1A). The daily mean $\Delta T_{leaf\text{-}air}$ of *Pinus* (1.17 ± 0.26 °C below air temperature) was significantly lower than that of *Pistacia, Quercus* and *Ceratonia* (3.30 ± 0.37, 2.71 ± 0.41 and 1.61 ± 0.27 °C above air temperature, respectively, p-value < 0.05). T_L values captured by the TIR camera were consistently ~3 °C warmer than T_L measured by the gas exchange chamber thermocouple for all species except for *Pinus*, where differences were larger (Fig. S4). These differences were associated with the fact that the thermocouple measurements were performed at ~1 m height, whereas the TIR-T_L measured the temperature at the canopy (2–12 m height), which was highest for the pine. Still, the good, positive and linear relationship between the methods supports the use of TIR sensing for T_L determination. The TIR images and the temperature density graphs, captured in the second day of measurements, illustrated the lower $\Delta T_{leaf\text{-}air}$ in conifers in comparison to the broadleaved species (Figs. 3B and 3C). The linear regression analysis of the relationship between E and $\Delta T_{leaf\text{-}air}$ yielded a negative correlation across four of the species (aside from *Quercus*; Fig. 3C).

3.2. Leaf temperature and transpiration in tree saplings in the greenhouse

The midday gas exchange measurements showed variations between tree species (Fig. 4). The conifers *Cupressus* and *Pinus* showed lower mean values of E (3.27 ± 0.7 and 5.21 ± 0.96 mmol H_2O m^{-2} s^{-1}, respectively) than the broadleaved *Quercus, Ceratonia* and *Pistacia* (5.65 ± 0.52, 7.02 ± 0.67, and 8.36 ± 0.77 mmol H_2O m^{-2} s^{-1}, respectively, p-value < 0.001). In contrary to field measurement in the forest, *Quercus* had lower values than either the conifer species. Stomatal conductance followed similar patterns, as would be expected under controlled conditions (Fig. 4B). *Cupressus* and *Pinus* showed lower g_s rates (0.09 ± 0.02 and 0.16 ± 0.04 mol H_2O m^{-2} s^{-1}, respectively) in comparison to *Quercus, Ceratonia* and *Pistacia* (0.22 ± 0.04, 0.31 ± 0.06, and 0.32 ± 0.04 mol H_2O m^{-2} s^{-1}, respectively, p-value < 0.001). In contrast, WUEi was higher for coniferous species, *Cupressus* and *Pinus* (93.37 ± 6.31 and 108.7 ± 6.45, respectively) than the broadleaves, *Quercus, Ceratonia* and *Pistacia* (50.87 ± 4.57, 38.79 ± 4.42 and 45.75 ± 2.1, respectively). Species differences in

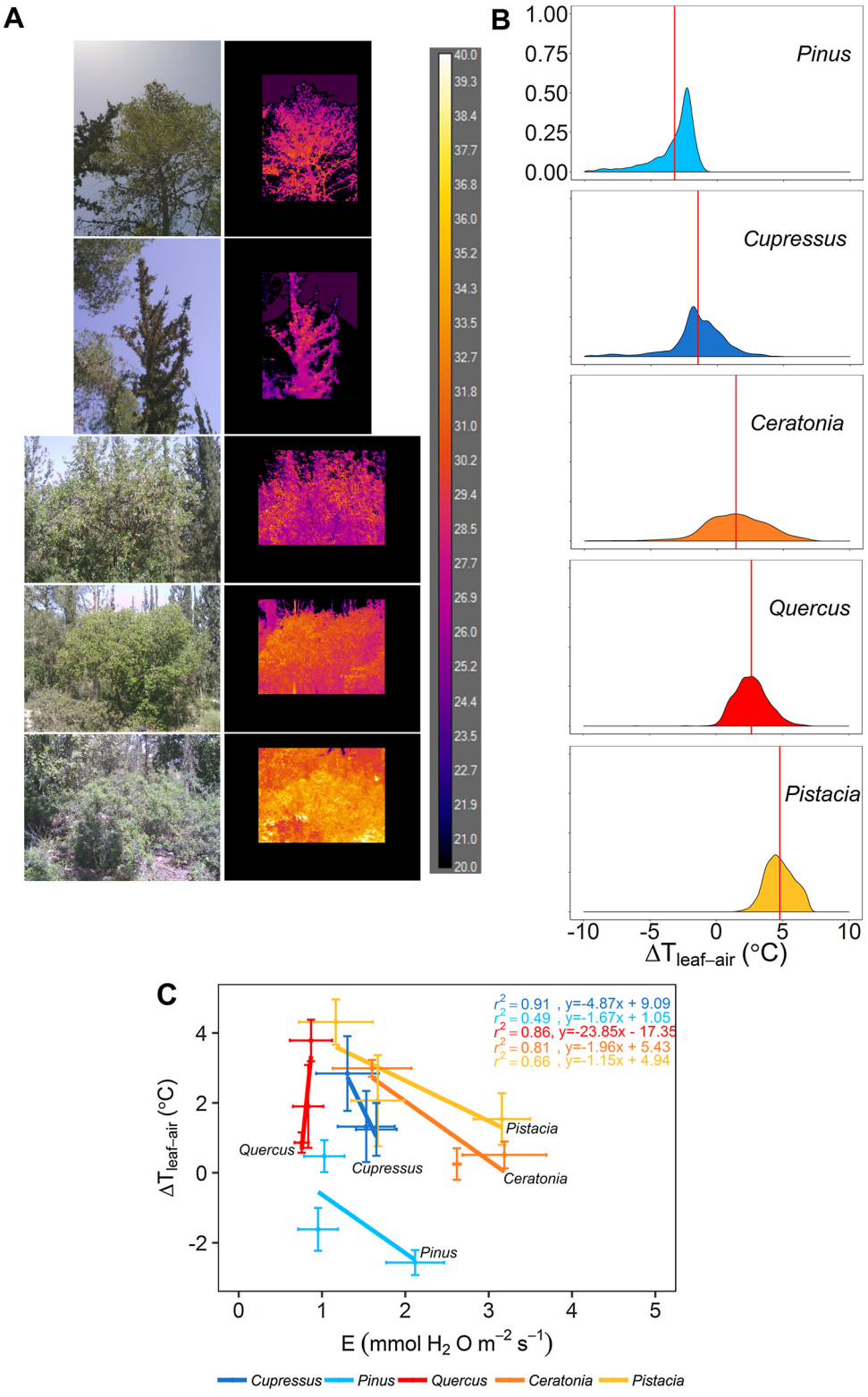

Fig. 3. TIR images and crown leaves' temperature distribution of five Mediterranean tree species. Images were taken on 26 March 2018 at midday. (A) Visible and false-colour TIR images of tree crowns (B) Probability density function (PDF) graphs of $\Delta T_{leaf\text{-}air}$ for each of the five tree species. Vertical red lines represent the mean canopy temperature. (C) Relationship between E and $\Delta T_{leaf\text{-}air}$ for sunlit leaves of the five tree species (For interpretation of the references to colour in this figure legend, the reader is referred to the web version of this article.).

WUEi (Fig. 4C) were larger than in E and g_s, probably due to the higher assimilation rates in the conifers (data not shown).

A total of four TIR images of the same five tree species were captured (Fig. S5). The averaged $\Delta T_{leaf\text{-}air}$ varied between the images; for example, the measured leaves in image #1 were warmer than the same leaves in image #4 by ~0.5-2.5 °C. However, across all four images, significant differences between tree species were evident (Kruskal-Wallis chi-squared = 9.93, df = 4, p-value < 0.05). The coniferous species were significantly cooler than the broadleaves (Welch's t test, t = 3.51, df = 15.66, p-value < .005). Leaf temperatures of *Pinus* and

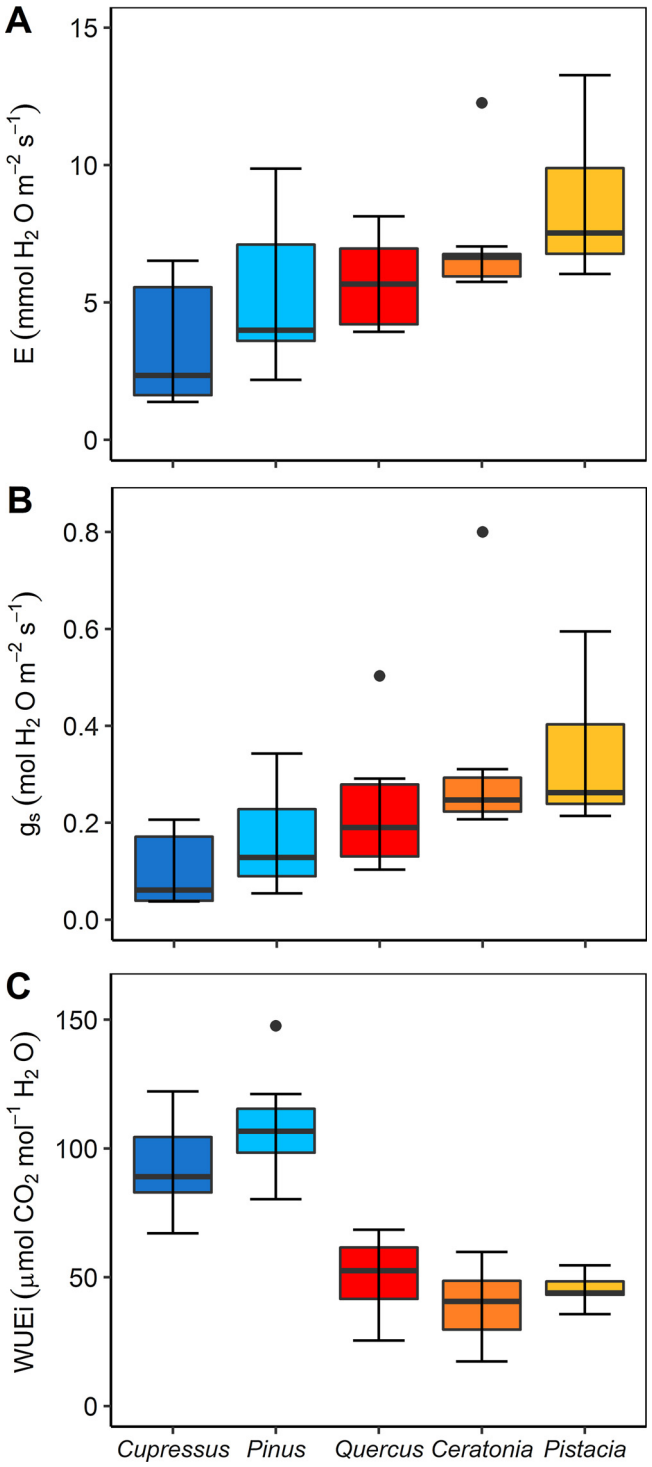

Fig. 4. Midday leaf gas exchange parameters of tree saplings. Transpiration rate (A), Stomatal conductance (B), Intrinsic water use efficiency (C) (n = 9). The different colours represent different tree species (*Cupressus sempervirens, Pinus halepensis, Quercus calliprinos, Ceratonia siliqua, Pistacia lentiscus*).

Cupressus showed maximum values of 1.10 °C and 1.49 °C above air temperature, respectively, while *Pistacia, Quercus* and *Ceratonia* showed values of 3.43 °C, 3.63 °C and 4.27 °C above air temperature, respectively. The $\Delta T_{leaf\text{-}air}$ distributions measured from TIR image #1 were further used to construct probability density functions (PDF; Fig. 5C). *Pinus* and *Cupressus* showed narrow temperature distributions, with relatively high values of kurtosis, 9.59 and 11.82, respectively. In contrast, *Pistacia, Quercus* and *Ceratonia* showed broad temperature

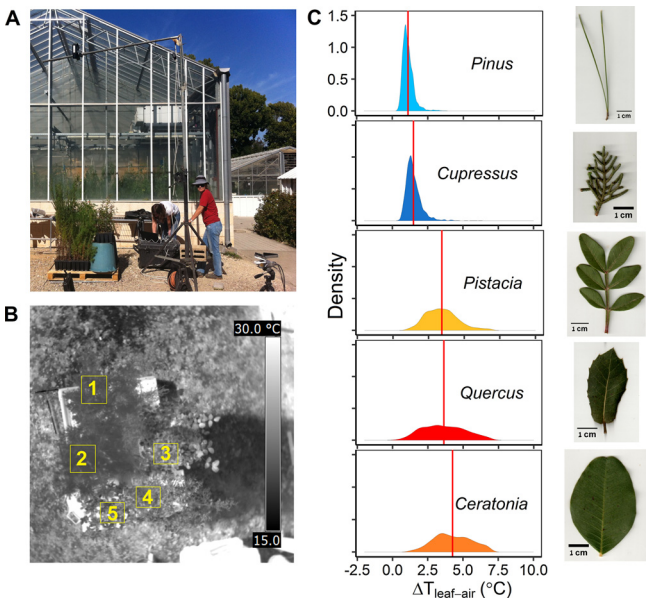

Fig. 5. (A) Experiment setup: one year-old tree saplings placed on a wood platform and an Infra-Red camera located at 2.8 m height above trees' canopies; (B) TIR image with selected region of interest (ROI) of species specific sunlit leaves: ROI 1 = *Cupressus sempervirens*, ROI 2= *Pinus halepensis*, ROI 3 = *Ceratonia siliqua*, ROI 4 = *Pistacia lentiscus*, ROI 5 = *Quercus calliprinos* ; (C) Probability density function (PDF) graphs of the five tree species, measured from the TIR image and leaf shape of the different tree species. Vertical red lines represent the mean canopy temperature (For interpretation of the references to colour in this figure legend, the reader is referred to the web version of this article.).

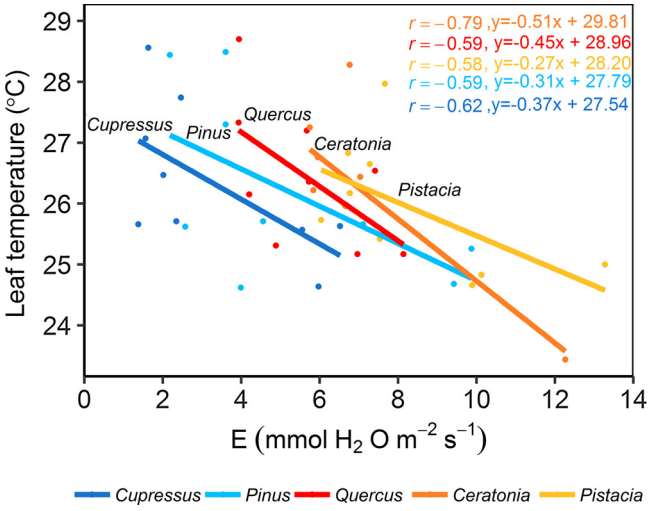

Fig. 6. Leaf-scale relationship between transpiration rate and leaf temperature of the five tree species. Measurements are based on saplings which were grown under sustained irrigation regime in a greenhouse (n = 9).

distributions, with relatively low values of kurtosis, 3.18, 2.24 and 2.27, respectively. The leaf-scale relationship between E and T_L showed a negative correlation among all species (Fig. 6). The different species showed similar regression lines with slopes ranging between -0.27 and -0.51 °C for respective increase of 1 mmol m^{-2} s^{-1} in E. r^2 values ranged between 0.33 to 0.62, with p-value < 0.1 (except for the p-value of 0.1 for *Pistacia*).

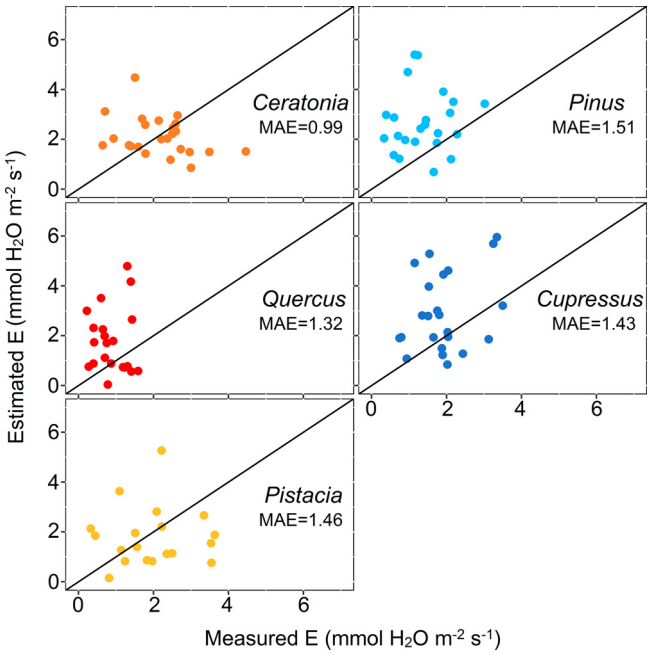

Fig. 7. Comparison between directly measured and modeled values of E. A 1:1 line indicates a full agreement between measured and modeled values.

3.3. Comparison between direct measurement and thermal-based estimation of transpiration rate

The measured E values from the forest measurements were plotted against estimated values of E, which were computed from the thermal images based on the leaf energy balance model (Fig. 7). A 1:1 line indicates a full agreement between measured (x-axis) and modeled (y-axis) values. Across the five tree species, the leaf energy balance model predicted E values at the correct range of 0–6 mmol H_2O m^{-2} s^{-1}. The mean absolute errors ranged between 0.99 to 1.51 mmol H_2O m^{-2} s^{-1}, where modeled values of *Ceratonia* showed the highest agreement and *Pinus* showed the poorest agreement with the direct measured values. In general, 66% of the total E values were above the 1:1 line, indicating that the predictions of the model tended toward overestimation.

4. Discussion

This study demonstrates a negative correlation between $\Delta T_{leaf\text{-}air}$ and E in coexisting, key tree species of the Mediterranean maquis. This was expected from the cooling effect that occurs as water evaporates and the vapor is transpired through the stomatal pores on the surface of the leaves (Gates, 1968). Leaf surface cooling requires sufficient soil water availability and high hydraulic conductivity. Therefore, in well-irrigated tree saplings growing under controlled conditions, the reduction in leaf surface temperature across the species was more robust than in the field, all else being equal. Urban et al. (2017) reported that the leaf temperatures of poplar in dry soil were an average of 1.1 °C cooler than non-transpiring leaves, while in wet soil, temperature differences reached up to 9 °C. TIR images of crown leaves indicated that coniferous species were significantly cooler than broadleaved species and temperature distribution varied between these two contrasting leaf types. These differences between conifers and broadleaves might be related to differences in leaf dimensions, which affect the actual wind speed and thickness of boundary layer around the leaf surface. In turn, these factors influence the boundary layer conductance to water vapor (g_{bv}) and heat transfer (g_{bH}). An increase in leaf size of broadleaved species diminishes g_{bv} and results in an increase in T_L (Taylor, 1975; Geller and Smith, 1982). In contrast, the small coniferous leaves are more tightly coupled to the surrounding air, characterized by large g_{bv} and g_{bH}, and therefore, T_L tends to be at or lower than air temperature (Jarvis and McNaughton, 1986; Martin et al., 1999). Fig. 5 confirms these theoretical considerations, by showing a mild increase in $\Delta T_{leaf\text{-}air}$ with leaf size among broadleaved saplings, from *Pistacia* to *Quercus* and to *Ceratonia*. It is interesting to note that the $\Delta T_{leaf\text{-}air}$ of broadleaved mature trees in the forest (Fig. 2) showed an opposite ranking (*Ceratonia* < *Quercus* < *Pistacia*). These differences highlight the important influence of tree height on $\Delta T_{leaf\text{-}air}$. According to wind profile relationship, the lowest wind speed is near the ground surface and it exponentially increases with height. As mentioned above, the wind speed has a significant role in heat transfer and that may explain why the 2-meter tall *Pistacia*, which normally grows close to the ground surface, had higher T_L than the other, taller tree species.

Leuzinger and Körner (2007) suggested that differences in T_L between coniferous and broadleaved species could not be explained only by leaf dimensions and stomatal conductance, but also and more importantly, by the influence of leaf and canopy structures (e.g., leaf canopy density, architecture, tree branching). These factors influence the turbulence and the penetration of airflow through the canopy and, in turn, affect the leaf boundary layer (Domingo et al., 1996). In general, trees with open, low density canopies should be cooler than trees with close, dense canopies. This idea is confirmed in Fig. 3, which demonstrates that among the broadleaved species, the $\Delta T_{leaf\text{-}air}$ of *Ceratonia*, characterized by a spreading crown, was cooler than the close, dense-foliaged *Quercus*. The relationship between E and $\Delta T_{leaf\text{-}air}$ of the mature trees, indicate evaporative cooling throughout the day in all studied tree species except in *Quercus* (Fig. 3C). The unusual result for *Quercus*, reflected in a positive correlation between E and $\Delta T_{leaf\text{-}air}$ might be related to exposure to direct sunlight. Surface leaf temperature is determined by the energy balance between the absorbed solar radiation and heat loss by evaporation and convection (Campbell and Norman, 1990; Jones, 1992). Gas exchange measurements showed that *Quercus* had relatively low E throughout the day (0.82 ± 0.1 mmol H_2O m^{-2} s^{-1}). In these low levels of E, the evaporative cooling effect in *Quercus* is smaller than the radiative heating and therefore $\Delta T_{leaf\text{-}air}$ increases.

Temperature distributions of the tree species indicated large variations between the two leaf types (Fig. 5). The tall, narrow temperature distribution of *Pinus* and *Cupressus* and the broad temperature distribution of *Pistacia, Quercus* and *Ceratonia* might be related to the stomatal pore distribution characterized by each of the leaf types. Conifers typically have uniform stomatal distribution and their stomatal pores are usually arranged in rows across the needle (Kouwenberg et al., 2003). In contrast, broad leaves are characterized by non-homogenous stomatal distribution. Slavík (1963) found that the E in the apical part of the leaf is 50–70% lower than that of the basal part. Similar, but less significant, differences were reported between the edges and the central part of the leaf (Garbe et al., 2002). Notably, the observed wide range of temperatures consequently has a low density of probability values. In this aspect, the likelihood of a wire thermocouple measurement, based on single contact point, to represent the mean leaf temperature is accordingly low. These findings, together with the low number of replications (n = 9) may further explain the moderate r^2 values produced in the gas exchange measurements (Fig. 6). Field leaf gas exchange measurement in mature trees (Fig. 1) indicated higher E values of *Pinus* than those of *Quercus* throughout daytime. We typically expect *Quercus* transpiration to be higher than *Pinus* because of higher water availability related to its deeper root system and its lower leaf water potential, but the opposite can also occur, especially in the wet season (Klein et al., 2013).

Estimations of E from the measured TL and based on the leaf energy balance model were compared to the observed E from leaf gas exchange measurements (Fig. 7). Overall, the modeled values were relatively close to the observed E, with some overestimations in the model. However, this comparison is not straightforward, mainly due to differences in the microclimatic conditions considered by each method. While gas exchange measurements are based on detection of H_2O mole

fractions in air flow coming out from a closed leaf chamber, the thermal imagery is based on detection of TIR radiation emitted from the leaf surface in an open environment. In previous study of Inoue et al. (1990) on cotton leaves, that examined a porometer-measured E values against the estimations of E from a similar leaf energy balance model, the measured E values were consistently higher than the modeled values. That study suggested overestimation as a result of higher air flow and drier air inside the closed cuvette of the porometer, than the ambient conditions. Ferraz et al. (2016), who compared between single leaf and whole-canopy gas exchange measurements of papaya leaves, reported that the whole-canopy E was approximately half of the single leaf E values. The study proposed that implication of E from single-leaf scale measurement to a whole-canopy scale is not appropriate. Values of E calculated from the TIR images of mature trees in Harel forest were closer to the 1:1 line for broadleaved *Ceratonia* than for *Pinus* needles. Since the leaf energy balance model was originally designed for broad leaves, this can be expected. These results may suggest that the simple leaf energy model has limited accuracy in predicting the E across the different species, and thus, species-specific adjustments are needed. At the same time, it demonstrated that chamber measurements are limited in representing the E of the whole canopy.

The tree saplings experiments and mature trees measurements in the forest, showed the diversity in $\Delta T_{leaf\text{-}air}$ among the different tree species, and in particular between conifers and broadleaves. This illustrates the potential influence of tree species composition on forest surface temperatures, and specifically for the Eastern Mediterranean, a warm oak-dominated maquis compared to a cool pine forest. Forest composition also has an important impact on local climate by determining the amount of solar radiation reaching the ground and the exchange of energy and water vapors with the atmosphere (Ellison et al., 2017). Therefore, an oak-dominated maquis, which is characterized by larger leaf area and closer, warmer canopies, is expected to have a stronger impact on the regional cooling than pine forests, similar to the effect shown in studies at the temperate zone (Renaud and Rebetez, 2009; Naudts et al., 2016).

Our study illustrates the use of TIR imagery in detection of transpiration-related differences in the natural environment. However, the dependence of $\Delta T_{leaf\text{-}air}$ in E has species-specific manner that might be related to differences in species' physiological traits such as leaf size and shape. These leaf-scale differences translate into tree-scale and species effects on the forest water balance, in turn affecting components of the hydrological cycle in forests (Klein et al., 2013). Therefore, capturing the levels of transpiration in multiple, coexisting tree species creates a novel approach to monitoring tree water-use *in situ*. Understanding species-specific patterns is the key for sustainable forest management in an uncertain future of land-use change and climate change. In conclusion, our observations highlight the necessity of high-resolution, large-scale surveys of leaf temperature using TIR imaging in forest research.

Acknowledgements

The authors would like to thank: (1) the Jewish National Fund (KKL) for providing the saplings for the greenhouse experiment (through the nursery in Eshtaol), and for permitting access to the study plot in Harel forest (through the forest management section); (2) The Weizmann campus greenhouse facility crew for greenhouse maintenance and support; (3) Prof. Dan Yakir (WIS) for providing the LiCor 6400 photosynthesis system; and (4) Zachary Gold Meital Tzandok for the proof reading.. TK wishes to thank the Merle S. Cahn Foundation and the Monroe and Marjorie Burk Fund for Alternative Energy Studies; Mr. and Mrs. Norman Reiser, together with the Weizmann Center for New Scientists; and the Edith & Nathan Goldberg Career Development Chair. The authors wish to thanks two anonymous reviewers for their useful comments, which have improved the quality of this paper.

Appendix A. Supplementary data

Supplementary material related to this article can be found, in the online version, at doi:https://doi.org/10.1016/j.agrformet.2019.02.014.

References

Alchanatis, V., Cohen, Y., Cohen, S., Moller, M., Sprinstin, M., Meron, M., Tsipris, J., Saranga, Y., Sela, E., 2010. Evaluation of different approaches for estimating and mapping crop water status in cotton with thermal imaging. Precis. Agric. 11, 27–41.
Aubrecht, D.M., Helliker, B.R., Goulden, M.L., Roberts, D.A., Still, C.J., Richardson, A.D., 2016. Continuous, long-term, high-frequency thermal imaging of vegetation: uncertainties and recommended best practices. Agric. For. Meteorol. 228–229, 315–326.
Bridge, L.J., Franklin, K.A., Homer, M., 2013. Impact of plant shoot architecture on leaf cooling: a coupled heat and mass transfer model. J. R. Soc. Interface 10, 20130326.
Burke, J.J., Upchurch, D.R., 1989. Leaf temperature and transpirational control in cotton. Environ. Exp. Bot. 29, 487–492.
Campbell, G.S., Norman, J.M., 1990. Estimation of plant water status from canopy temperature: an analysis of the inverse problem. In: Steven, M.D., Clark, J.A. (Eds.), Applications of Remote Sensing in Agriculture. Butterworths, London, pp. 255–271.
Cohen, Y., Alchanatis, V., Meron, M., Saranga, Y., Tsipris, J., 2005. Estimation of leaf water potential by thermal imagery and spatial analysis. J. Exp. Bot. 56, 1843–1852.
Danin, A., 1988. Flora and vegetation of Israel and adjacent areas. In: Yom-Tov, Y., Tchernov, E. (Eds.), The Zoogeography of Israel. Springer, Netherlands, pp. 251–276.
Domingo, F., Van Gardingen, P.R., Brenner, A.J., 1996. Leaf boundary layer conductance of two native species in Southeast Spain. Agric. For. Meteorol. 81, 179–199.
Ellison, D., Morris, C.E., Locatelli, B., Sheil, D., Cohen, J., Murdiyarso, D., Gaveau, D., 2017. Trees, forests and water: cool insights for a hot world. Glob. Environ. Change 43, 51–61.
Ferraz, T.M., Rodrigues, W.P., Netto, A.T., de Oliveira Reis, F., Peçanha, A.L., de Assis Figueiredo, F.A.M.M., de Sousa, E.F., Glenn, D.M., Campostrini, E., 2016. Comparison between single-leaf and whole-canopy gas exchange measurements in papaya (Carica papaya L.) plants. Sci. Hortic. (Amsterdam) 209, 73–78.
Froux, F., Ducrey, M., Dreyer, E., Huc, R., 2005. Vulnerability to embolism differs in roots and shoots and among three Mediterranean conifers: consequences for stomatal regulation of water loss? Trees - Struct. Funct. 19, 137–144.
Fuchs, M., 1990. Infrared measurement of canopy temperature and detection of plant water stress. Theor. Appl. Climatol. 42, 253–261.
Fuchs, M., Tanner, C.B., 1966. Infrared thermometry of vegetation1. Agron. J. 58, 597.
Garbe, C., Schurr, U., Jaehne, B., 2002. Thermographic measurements on plant leaves. Thermosense XXIV. Proc. SPIE 4710, 407–417.
Gates, D.M., 1968. Transpiration and leaf temperature. Annu. Rev. Plant Physiol. 19, 211–238.
Geller, G.N., Smith, W.K., 1982. Influence of leaf size, orientation, and arrangement on temperature and transpiration in three high-elevation, large-leafed herbs. Oecologia 53, 227–234.
Giorgi, F., 2006. Climate change hot-spots. Geophys. Res. Lett. 33, L08707.
Goubanova, K., Li, L., 2007. Extremes in temperature and precipitation around the Mediterranean basin in an ensemble of future climate scenario simulations. Glob. Planet. Change 57, 27–42.
Idso, S.B., Jackson, R.D., Ehrler, W.L., Mitchell, S.T., 1969. A method for determination of infrared emittance of leaves. Ecology 50, 899–902.
Idso, S.B., Jackson, R.D., Pinter, P.J., Reginato, R.J., Hatfield, J.L., 1981. Normalizing the stress-degree-day parameter for environmental variability. Agric. For. Meteorol. 24, 45–55.
Inoue, Y., Kimball, B.A., Jackson, R.D., Pinter, P.J., Reginato, R.J., 1990. Remote estimation of leaf transpiration rate and stomatal resistance based on infrared thermometry. Agric. For. Meteorol. 51, 21–33.
Inoue, Y., Sakuratani, T., Shibayama, M., Morinaga, S., 1994. Remote and real-time sensing of canopy transpiration and conductance-comparison of remote and stem flow gauge methods in soybean canopies as affected by soil water status. Japan J. Crop Sci. 63, 664–670.
Irmak, S., Haman, D.Z., Bastug, R., 2000. Determination of crop water stress index for irrigation timing and yield estimation of corn. Agron. J. 92, 1221–1227.
Jackson, R.D., Idso, S.B., Reginato, R.J., Pinter, P.J., 1981. Canopy temperature as a crop water stress indicator. Water Resour. Res. 17, 1133–1138.
Jarvis, P.G., Mcnaughton, K.G., 1986. Stomatal control of transpiration: scaling up from leaf to region. Adv. Ecol. Res. 15, 1–49.
Jones, H.G., 1992. Plants and Microclimate: A Quantitative Approach to Environmental Plant Physiology. Cambridge university press.
Jones, H.G., 1999a. Use of infrared thermometry for estimation of stomatal conductance as a possible aid to irrigation scheduling. Agric. For. Meteorol. 95, 139–149.
Jones, H.G., 1999b. Use of thermography for quantitative studies of spatial and temporal variation of stomatal conductance over leaf surfaces. Plant Cell Environ. 22, 1043–1055.
Jones, H.G., Archer, N., Rotenberg, E., 2004. Thermal radiation, canopy temperature and evaporation from forest canopies. For. Land-Atmosph. Interface 123–144.
Jones, H.G., Hutchinson, P.A., May, T., Jamali, H., Deery, D.M., 2018. A practical method using a network of fixed infrared sensors for estimating crop canopy conductance and evaporation rate. Biosyst. Eng. 165, 59–69.
Kim, Y., Still, C.J., Hanson, C.V., Kwon, H., Greer, B.T., Law, B.E., 2016. Canopy skin

temperature variations in relation to climate, soil temperature, and carbon flux at a ponderosa pine forest in central Oregon. Agric. For. Meteorol. 226–227, 161–173.
Kim, Y., Still, C.J., Roberts, D.A., Goulden, M.L., 2018. Thermal infrared imaging of conifer leaf temperatures: comparison to thermocouple measurements and assessment of environmental influences. Agric. For. Meteorol. 248, 361–371.
Klein, T., Cohen, S., Yakir, D., 2011. Hydraulic adjustments underlying drought resistance of Pinus halepensis. Tree Physiol. 31, 637–648.
Klein, T., Shpringer, I., Fikler, B., Elbaz, G., Cohen, S., Yakir, D., 2013. Relationships between stomatal regulation, water-use, and water-use efficiency of two coexisting key Mediterranean tree species. For. Ecol. Manage. 302, 34–42.
Kouwenberg, L.L.R., McElwain, J.C., Kürschner, W.M., Wagner, F., Beerling, D.J., Mayle, F.E., Visscher, H., 2003. Stomatal frequency adjustment of four conifer species to historical changes in atmospheric CO2. Am. J. Bot. 90, 610–619.
Lavorel, S., Canadell, J., Rambal, S., Terradas, J., 1998. Mediterranean terrestrial ecosystems: research priorities on global change effects. Glob. Ecol. Biogeogr. Lett. 7, 157.
Leinonen, I., Grant, O.M., Tagliavia, C.P.P., Chaves, M.M., Jones, H.G., 2006. Estimating stomatal conductance with thermal imagery. Plant Cell Environ. 29, 1508–1518.
Leuzinger, S., Körner, C., 2007. Tree species diversity affects canopy leaf temperatures in a mature temperate forest. Agric. For. Meteorol. 146, 29–37.
Lima, R.S.N., García-Tejero, I., Lopes, T.S., Costa, J.M., Vaz, M., Durán-Zuazo, V.H., Chaves, M., Glenn, D.M., Campostrini, E., 2016. Linking thermal imaging to physiological indicators in Carica papaya L. under different watering regimes. Agric. Water Manag. 164, 148–157.
Martin, T.A., Hinckley, T.M., Meinzer, F.C., Sprugel, D.G., 1999. Boundary layer conductance, leaf temperature and transpiration of Abies amabilis branches. Tree Physiol. 19, 435–443.
Meron, M., Sprintsin, M., Tsipris, J., Alchanatis, V., Cohen, Y., 2013. Foliage temperature extraction from thermal imagery for crop water stress determination. Precis. Agric. 14, 467–477.
Möller, M., Alchanatis, V., Cohen, Y., Meron, M., Tsipris, J., Naor, A., Ostrovsky, V., Sprintsin, M., Cohen, S., 2007. Use of thermal and visible imagery for estimating crop water status of irrigated grapevine. J. Exp. Bot. 58, 827–838.
Naudts, K., Chen, Y., McGrath, M.J., Ryder, J., Valade, A., Otto, J., Luyssaert, S., 2016. Europe's forest management did not mitigate climate warming. Science 351 (6273), 597–600.
Reinert, S., Bögelein, R., Thomas, F.M., 2012. Use of thermal imaging to determine leaf conductance along a canopy gradient in European beech (Fagus sylvatica). Tree Physiol. 32, 294–302.
Renaud, V., Rebetez, M., 2009. Comparison between open-site and below-canopy climatic conditions in Switzerland during the exceptionally hot summer of 2003. Agric. For. Meteorol. 149 (5), 873–880.
R Core Team, 2013. R: A Language and Environment for Statistical Computing. ISBN 3-900051-07-0, URL. R Foundation for Statistical Computing, Vienna, Austria. http://www.R-project.org/.
Scherrer, D., Bader, M.K.F., Körner, C., 2011. Drought-sensitivity ranking of deciduous tree species based on thermal imaging of forest canopies. Agric. For. Meteorol. 151, 1632–1640.
Schindelin, J., Arganda-Carreras, I., Frise, E., Kaynig, V., Longair, M., Pietzsch, T., Preibisch, S., Rueden, C., Saalfeld, S., Schmid, B., Tinevez, J.Y., White, D.J., Hartenstein, V., Eliceiri, K., Tomancak, P., Cardona, A., 2012. Fiji: an open-source platform for biological-image analysis. Nat. Methods.
Schymanski, S.J., Or, D., Zwieniecki, M., 2013. Stomatal control and leaf thermal and hydraulic capacitances under rapid environmental fluctuations. PLoS One 8 (1), e54231.
Singer, A., 2007. The Soils of Israel. Springer Science & Business Media.
Slavík, B., 1963. The distribution pattern of transpiration rate, water saturation deficit, stomata number and size, photosynthetic and respiration rate in the area of the tobacco leaf blade. Biol. Plant. 5, 143–153.
Smigaj, M., Gaulton, R., Suarez, J.C., Barr, S.L., 2017. Use of miniature thermal cameras for detection of physiological stress in conifers. Remote Sens. 9, 957.
Tanner, C.B., 1963. Plant temperatures 1. Agron. J. 55, 210–211.
Taylor, S.E., 1975. Optimal leaf form. Perspectives of Biophysical Ecology. pp. 73–86.
Trifilò, P., Nardini, A., Gullo, M.A.L., Barbera, P.M., Savi, T., Raimondo, F., 2015. Diurnal changes in embolism rate in nine dry forest trees: relationships with species-specific xylem vulnerability, hydraulic strategy and wood traits. Tree Physiol. 35, 694–705.
Urban, J., Ingwers, M.W., McGuire, M.A., Teskey, R.O., 2017. Increase in leaf temperature opens stomata and decouples net photosynthesis from stomatal conductance in Pinus taeda and Populus deltoides x nigra. J. Exp. Bot. 68, 1757–1767.